Cubically cage-shaped mesoporous ordered silica for simultaneous visual detection and removal of uranium ions from contaminated seawater

Dina A. Tolan, [a,b] ***Emad A. Elshehy,*** [c,*] ***Waleed A. El-Said,*** [d,e] ***Tetsuya Taketsugu,*** [f,g] ***Kazunari Yoshizawa,*** [h] ***Ahmed M. El-Nahas,*** [a] ***Ali Reza Kamali,*** [I] ***and Amr M. Abdelkader*** [k,*]

[a]*Department of Chemistry, College of Science and Humanities, Prince Sattam bin Abdulaziz University, Alkharj 11942, Saudi Arabia*
[b]*Chemistry Department, Faculty of Science, Menoufia University, Menoufia, Egypt*
[c]*Nuclear Materials Authority, El Maadi, Cairo, Egypt*
[d]*Department of Chemistry, Faculty of Science, Assiut University, Assiut, 71516, Egypt*
[e]*University of Jeddah, College of Science, Department of Chemistry, P.O. Box 80327, Jeddah 21589, Saudi Arabia*
[f]*Department of Chemistry, Faculty of Science, Hokkaido University, Sapporo 060-0810, Japan*
[g]*Institute for Chemical Reaction Design and Discovery (WPI-ICReDD), Hokkaido University, Sapporo 060-0810, Japan*
[h]*Institute for Materials Chemistry and Engineering, Kyushu University, Nishi-ku, Fukuoka 819-0395, Japan*
i Energy and Environmental Materials Research Centre (E2MC), School of Metallurgy, Northeastern University, Shenyang, 110819, People's Republic of China
[k]*Department of Engineering, Bournemouth University, Talbot Campus, Fern Barrow, Poole, BH12 5BB, United Kingdom.*

**Corresponding authors: Amr Abdelkader(aabdelkader@bournemouth.ac.uk, aa494@cam.ac.uk)*
Emad Elshehy (eelshehy@yahoo.com)

Abstract

There is an increasing interest in developing new technologies enabling the efficient detection and removal of radioactive pollution from seawater. Here, we report a dual-function organic-inorganic mesoporous structure for naked-eye detection and removal of uranyl ions from an aqueous environment. The mesoporous sensor/adsorbent is fabricated via direct template synthesis of highly ordered silica monolith (HOM) starting from a quaternary microemulsion liquid crystalline phase. The produced HOM is subjected to further modifications through growing an organic probe, Omega Chrome Black Blue G (OCBBG), in the cavities and on the outer surface of the silica structure. The spectral response for [HOM-OCBBG→U(VI)] complex shows a maximum reflectance at λ_{max} = 548 nm within 1 min response time (t_R); the LOD is close to 9.1 µg/L while the LOQ approaches 30.4 µg/L, this corresponds to the range of concentration where the signal is linear against U(VI) concentration (i.e., 5 to 1000 µg/L) at pH 3.4 with standard deviation(SD) of 0.079 (RSD% = 11.7 at n=10). Experiments and DFT calculations indicate the existence of strong binding energy between the organic probe and uranyl ions forming a complex with blue color that can be detected by naked eyes even at low uranium concentrations. With regard to the radioactive remediation, the new mesoporous sensor/captor is able to reach a maximum capacity of 95 mg/g within a few

minutes of the sorption process. The synthesized material can be regenerated using simple leaching and re-used several times without a significant decrease in capacity.

Keywords: high order silica; radioactive pollution; nuclear waste; mesoporous materials; Sensor; chromogenic probs; adsorption

1. Introduction

Pollution from uranium species has turned out a global concern due to the rapid growth of nuclear technology during the last century. This species could be found in different accessible resources, such as uranium mining and processing, medical devices, glass manufacturing, and nuclear technologies, which all share a significant hazard to human health and pose a threat to the sustainability of the ecological environment and clean energy [1-6]. Therefore, developing simple and inexpensive technologies to detect and remove uranium from contaminated aqueous environments is essential. However, in the current technology, the detection is separated from the removal processes, adding more time and cost to the remediation processes, and most importantly, increasing the risk of exposure. Chemosorption techniques are at the forefront of the large-scale removal methods while detecting radionuclides is dominated by instrumental spectroscopic methods, such as Raman, atomic absorption, and atomic emission spectroscopy. There are, however, recent interest in the development and design of chemical sensors for the detection and quantifying radionuclides in natural water that offer good sensitivity, short response times, and selectivity [7-12]. Unfortunately, most sensors developed so far were kinetically slow with limited sensitivity, and the materials used to fabricate the sensor are different from those used for the removal. Therefore, there is a solid motivation to develop new materials that selectively capture and recognize uranium from contaminated water.

There are several attempts in the literature to design materials for the concurrent selective removal and detection of chemical molecules, especially for metal ions with industrial and environmental interests.[3] One of the most promising design concepts is based on introducing receptor subunits (binding sites) and chromogenic signalling stimulus into nano-channels of solid carriers. [13-15]

Many chromogenic reagents are available on-shelf, increasing the opportunities to select the proper probes corresponding to a particular sensing application according to its spectroscopic properties and chemical reactivity [16-18]. Azo-dyes are among the chromogenic reagents widely used for the spectrophotometric detection of uranyl

ions [18-20]. Liang et al. combined arsenazo III dye with gold nanoparticles and fabricated a new sensor for selective detection of uranyl ions [21]. The mono azo-dye omega chrome black G is widely used as an indicator for the volumetric determination of some metal ions [22]. To the best of our knowledge, no studies have applied omega chrome black G as a chemosensor for the visual detection of uranium from aqueous solutions.

Organic-inorganic hybrid materials are promising candidates as active materials for the chemical sensing and sorption processes from aqueous solutions because of their chemical and thermal stability, large specific surface area, and low toxicity to the aqueous environment. These structures combine the advantages of both organic and inorganic materials, allowing tuning their chemical, physical and morphological properties [23-26]. These structures' surface functionalizations can provide interesting chemical and physicochemical properties, enabling effective uranium treatment in complex environments [27-29]. Mesoporous silica material with pores diameters in the range of 2-50 nm exhibits important advantages such as large surface area, well-defined pore size, chemical stability, and easy modification. These characteristics make mesoporous silica ideal matrix to co-host chromogenic chemosensors and active sorbents, enabling the simultaneous detection and separation of uranium [30, 31]. Chromogenic receptors are usually covalently bonded to mesoporous silica surfaces either through co-condensing of the functional moieties during the framework cross-linking or post-grafting after the framework formation. As such, this harmonic design results in surface functionalization/intercalation of a chromogenic probe into the silica network with well-defined cages or cylindrical pores. These unique features allow tunning the performance of silica-based organic-inorganic hybrids towards developing dual-functional materials that can remove target ions and provide sensing capability to detect the target ions [32].

Herein, we report a hierarchal mesoporous captor/sensor based on cubical silica as sponge scaffold anchored with OCBBG (containing different donor atoms like nitrogen, oxygen and sulfur) receptor for combined recognition and removal of uranium from contaminated media. The mesocaptor responses can be triggered by uranyl ions and transduce measurable signals at synergistic pH value, which enable binding of uranyl ions into the hydrophobic organic probe loaded into the cubical cage-shaped mesoporous ordered silica. The adsorption behavior of the mesoporous captor/sensor towards U(VI) is investigated at different experimental conditions. The sensor-to-U(VI) interaction mechanism is explored further by DFT calculations. Finally, the application of the modified silica materials for selective separation of U(VI) from contaminated real seawater samples is demonstrated.

2. Materials and Methods

2.1 Materials

Tetramethyl orthosilicate (TMOS), the triblock copolymers of poly(ethylene oxide-b-propylene oxide-b-ethylene oxide) pluronic F108 [F108 ($EO_{141}PO_{44}EO_{141}$)], Omega Chrome Black Blue G (OCBBG) were purchased from Sigma–Aldrich Company Ltd. (USA). Buffer solutions (0.2 M) KCl–HCl and (0.2 M) CH_3COOH-CH_3-COONa (acetate) were used for the pH adjustments during the detection process in the 1–6 range (ADWIC, Egypt). 3-morpholinopropane sulfonic acid (MOPS)-NaOH was used for the pH adjustments during the detection process. $UO_2(NO_3)_2 \cdot 6H_2O$ was used as a source of U(VI). Other chemicals were received from ADWIC, Egypt.

2.2 Fabrication of optical mesosensor

Hierarchal high ordered mesoporous (HOM) monoliths were synthesized via the direct templating method described elsewhere using the lyotropic liquid crystalline phase of pluronic F108 as the template [31] (see the Supporting Information file). The HOM-OCBBG mesoporous sensor/captor was fabricated via a direct immobilization method. First, 0.1 M acetone solution of OCBBG and 0.5 g of HOM material were mixed. The immobilization procedure was performed under vacuum at 45°C until probe saturation was achieved. Next, the acetone was removed using a gentle vacuum connected to a rotary evaporator at room temperature, leading to the dye probe's direct interaction with the mesoporous HOM composite. The HOM-OCBBG sensor/captor wrapping step was repeated several times until the probe molecules' equilibrium (adsorption capacity) was detected spectrophotometrically as saturated. Upon reaching saturation, the fabricated mesoporous sensor/captor was thoroughly washed with deionized water until no probe elution was observed. The washed sensor/captor was then dried at 65°C for 2 h. The resulting mesoporous sensor/captor was then dried at 65°C to 70°C for 3 h to 4 h and ground into a fine powder before removing/detecting U(VI) ions.

2.3 Sensor workability for U(VI) ions detection

The optical sensing of the U(VI) ions using HOM-OCBBG sensor/captor was performed by adding solution with specific concentrations of U(VI) ions (adjusted at appropriate pH of 3.4 (KCl/HCl) at constant volume (20 mL) and 20 mg of HOM-OCBBG sensor/captor with shaking in a temperature-controlled water bath with a mechanical shaker at 25 °C for 20 min at a constant agitation speed of 300 rpm to achieve good color development. A blank solution was also prepared, following the same procedures for comparison. The HOM-OCBBG sensor/captor was then collected by suction through a 25 mm diameter cellulose acetate filter paper. The collected sensor/captor on the cellulose acetate filter paper was estimated qualitatively by the naked eye and quantitatively by reflectance

spectroscopy. The solution's U(VI) concentration was analyzed using ICP-MS before and after recognition by the microporous cellulose acetate filter paper. Successive measurements were performed using wide-range concentrations of standard "known" solutions of U(VI) to ensure both accuracy and the precision of U(VI) ions sensing system in seawater and real uranium waste leach liquor. The calculated standard deviation of U(VI) ions concentrations was 0.05%. The detection range (D_R), the limit of detection (LOD), and the limit of quantification (QOD) of U(VI) ions with the use of the HOM-OCBBG sensor/captor were estimated from the linear part of the calibration plot based on the following eqs. (1&2) [10];

$$LOD = 3S_b/m \quad (1)$$

$$QOD = 10S_b/m \quad (2)$$

where k = 3 or 10 for both LOD and QOD, respectively, S_b is the standard deviation, and m is the slope of the linear portion of the calibration curve.

3. Results and discussion

3.1 Materials Characterization

Mesocage cubic Im3m (HOM) mesostructured carriers with uniform cavities and entrance pores were fabricated using the direct templating method. Scanning electron microscopy (SEM) of the hierarchal HOM-OCBBG sensor/captor clearly showed the formation of micrometric particles. The host HOM monolith's particle size could be estimated to be about 650-900 nm, as seen in the SEM images (Fig. S1). HRTEM micrographs of nanostructured material produced before and after the interaction of HOM-OCBBG with U(VI) species are shown in Fig. 1. Figure (1A&B) provides evidence for forming 3D cubically caged mesoporous Im3m structures. The small-angle XRD (SAX) analysis shows the well-ordered mesopore architectures along the [100] direction is evidenced from the small-angle XRD (SAX) analysis. The SAX pattern (Fig. S1(B)) of mesocage silica carrier showed a broad diffraction peak in the range of $0.9 < 2°\theta < 3.0$, indicating the formation of cubic Im3m monoliths. Depositing OCBBG within the silica pores reduces the space inside the meso-architectured pores (Fig. 1C&D). The HRTEM images (Fig. 1(C&D) revealed the retention of the mesostructured pore cages after embedding the OCBBG moieties. Only a slight distortion in the size of pores and spherical cavities can be observed, as evidenced by the formation of multi-directional zigzag channels. Both TEM images and elemental mapping (Fig. S2) indicate that the organic probe is uniformly distributed within the cage cavities and coated on the surface, leading to the hierarchal porous structure formation HOM-OCBBG. The EDX analysis shows that both Si and O are synchronized together, while C,

N, and S exist side-by-side, indicating the direct immobilization of OCBBG ligand in and on the host monolith. A more detailed analysis of the chemical composition of the surface of HOM-OCBBG and the presence of uranyl ions by elemental mapping taken with energy dispersive X-ray (EDX) is shown in Fig. 2. The carbon and oxygen corresponding micrographs for the two samples (HOM-OCBBG and HOM-OCBBG/UO_2 show that Si and O are forming the substrate, while the carbon, nitrogen, and sulfur micrographs indicate the distribution of the organic probe formed on the surface. The presence of uranyl ions adsorbed on HOM-OCBBG also shows a uniform distribution. Figure 1 (E&F) of HRTEM micrographs after HOM-OCBBG of U(VI) species, indicating that the distortion of pores in HOM- OCBBG sensor/captor leads to the formation of selective sensing and capturing sites for U(VI) among competitive ions. The analysis of HOM-OCBBG/UO_2 shows that the amount of interacted uranium ions is proportional to the amount of nitrogen present.

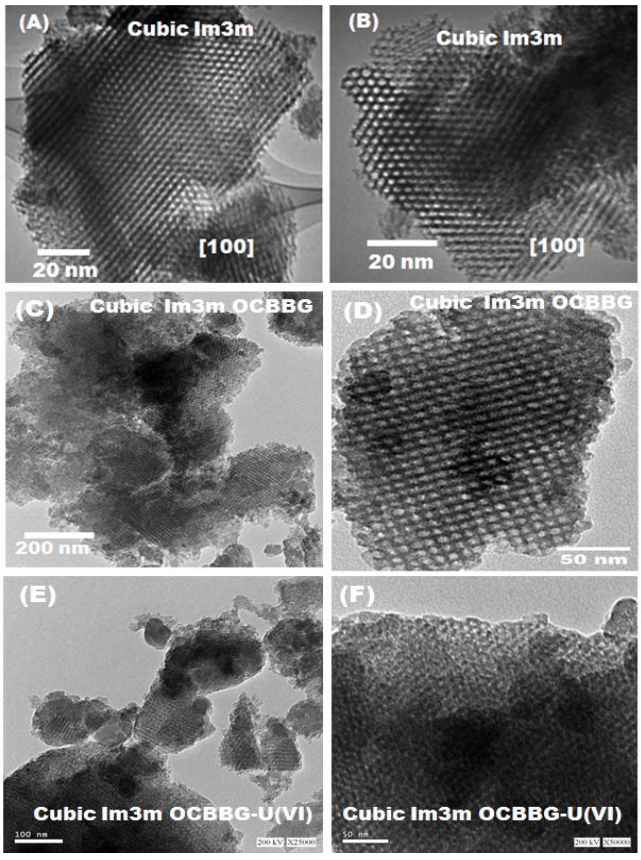

Fig. 1 (A&D) HRTEM micrographs of HOM fabricated via direct template synthesis, (C&D) HRTEM micrographs of OCBBG and (E&F) HRTEM micrographs of HOM- OCBBG after complexation with of U(VI) species.

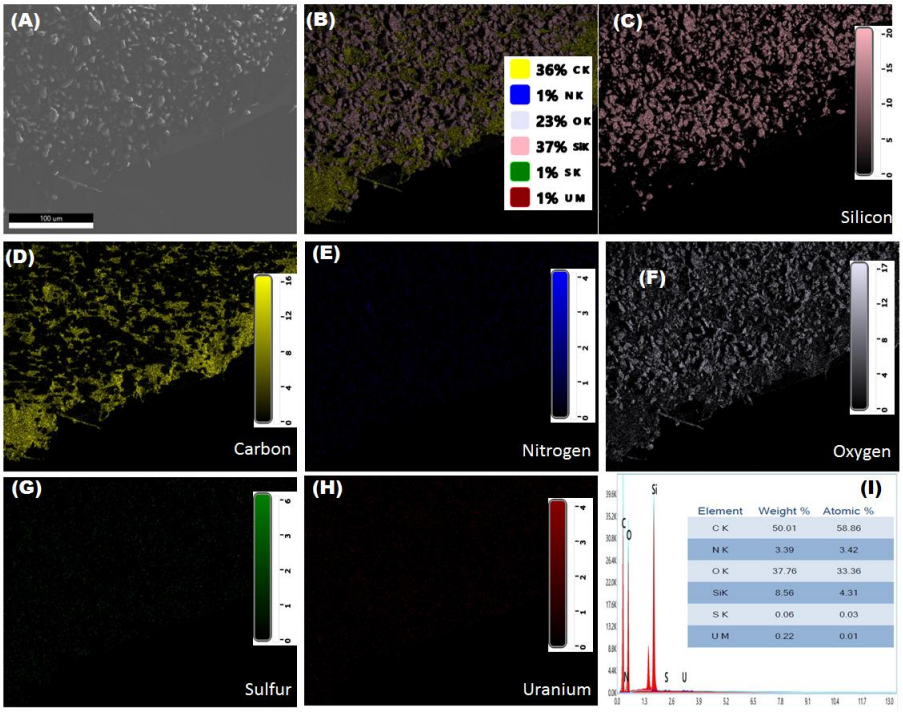

Fig. 2 SEM image and elemental mapping of meso-caged HOM-OCBBG sensor/captor after uranyl ion interaction.

The N_2 isotherms provide further evidence of the shape- and size-controlled cubic mesostructured monoliths. As seen from Fig. 3(A), the nitrogen adsorption/desorption isotherm of the free HOM and HOM-OCBBG exhibit typical "type IV" isotherms with H3 hysteresis loops, indicating mesoporous structures. After loading OCBBG, the hysteresis loops shift to higher relative pressure ($P/P_0 \geq 0.45$) with some reduction in the hysteresis loop's width, implying lower porosity. The calculated BET-specific surface area of the HOM carrier is 412 m^2/g, and the average pore diameter is 18.5 nm (See Figure S1(C), Supporting Information. The decrease in surface area and pore volume upon immobilization of OCBBG (i.e. 335.53 m^2/g and 0.7627 cm^3/g, respectively) proves the OCBBG probe's inclusion inside the cage cavities. Despite the slight reduction, the monolith's large initial surface area satisfied the large specific surface area after embedding the organic probes pore. These confined pores are beneficial for capturing and detecting ultra-trace amounts of the target ions, as will be discussed later.

The FT-IR spectra (Fig. 3(B)) provides evidence for the successful functionalization of the HOM-Si. The FT-IR spectrum of silica monoliths displays several characteristic bands, within which the strong band at 1090 cm^{-1} is related to υ(Si-O-Si) of siloxane backbone, the band at 804 cm^{-1} corresponds to the tetrahedron ring in (SiO_4) [32]. After anchoring the organic probes, the HOM-OCBBG spectrum shows several new bands in the range of 1200-3200 $cm^{-1,}$ including the one related to the N–H stretching around 3300 cm^{-1} overlapping with the (Si–OH) and C–H

stretching bands at 3100 and 2977 cm^{-1}, respectively, and those of amide I [C=O stretching + C-N stretching] at 1635 cm^{-1}, amide II [N–H bending + C-N stretching] at 1490 cm^{-1}, amide III (N–H deformation + C-N stretching) at 1370 cm^{-1} and υ(C-S) at 690 cm^{-1} [33-36]. The silica characteristic peaks' intensity was significantly reduced after anchoring OCBBG in/on the HOM cavities and surface. Also, the broadband at ~3400 cm^{-1} corresponding to the O-H stretching vibration decreased after the OCBBG functionalization, indicating a significant reduction in the physically adsorbed water. The dynamic light scattering (DLS) curve (Fig. S1(D)) shows two prominent peaks, one centered at 900 nm and one at 65 nm, indicating the dual-phase nature of the HOM-OCBBG mesosensor. Moreover, the zeta potential analysis displays the homogenous distribution of the charge of anionic nanoparticles, with highly negative zeta potential (i.e., close to -21.9 mV) (Fig. S1(E)). This is an important criterion to consider for interpreting both the type of the organic ligand and the shape of particles. In addition, this global anionic charge can explain the limited aggregation of nanoparticles, which is also essential for adequately structuring the material during synthesis.

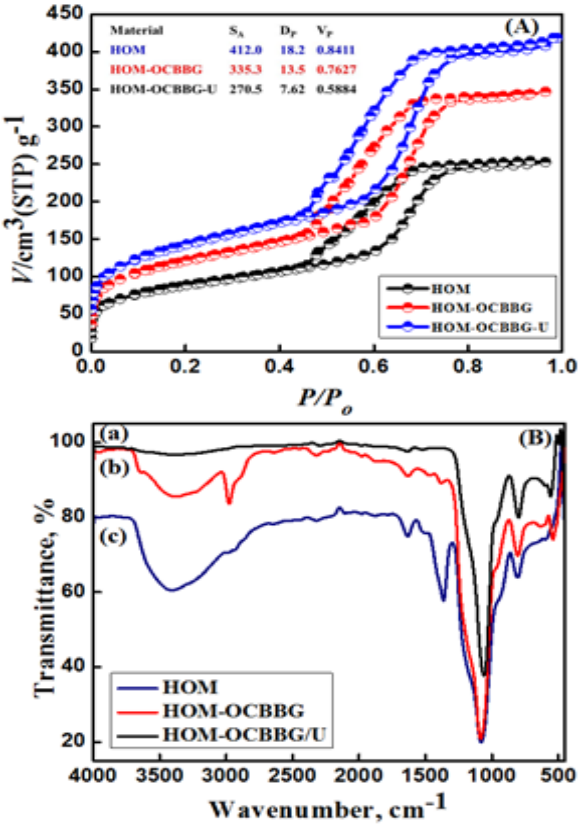

Fig 3: (A) N_2 adsorption-desorption isotherms and (B) FTIR spectra for fabricated MOH-Si, MOH-OCBBG, and HOM-OCBBG after U(VI) ions capturing.

3.2. Uranyl ions adsorption assays

The ability of HOM-OCBBG on detecting and remove U(VI) was assessed through quantitative and qualitative studies at different pH values (Fig. 4). The prominent color change and signal saturation in the reflectance spectra of the sensor were recorded after *tR*. In a solid-state ion-sensing system, the sensor is strongly sensitive in its optical "color intensity" and signal responses toward the pH of a solution containing U(VI) ions. The notable fast changes in the color and reflectance intensity of the U(VI) sensor can be clearly observed at the pH value of 3.4. The changes in color and reflectance spectra indicate a fast and strong interaction of U(VI) and OCBBG forming $[U\text{-}OCBBG]^{n+}$ complex (Fig. 4(A). U(VI) highest uptake value is about 95 mg/g, measured at the same pH value of 3.4 (Fig. 4(B)). It has been reported that in acidic solution (pH solution < 3), uranium exists as dioxo uranyl cation UO_2^{2+}, while hydroxo complexes of uranium dominate at higher pH [37]. These species of uranyl hydroxo complexes comprise $UO_2(OH)^+$, $(UO_2)_2(OH)_2^{2+}$, $(UO_2)_3(OH)^{5+}$ and $(UO_2)_4(OH)^{7+}$, with their concentrations varying with pH solution [38, 39]. The dominant uranium species at pH 7 is $(UO_2)_3(OH)^{5+}$ with approximately 74.5% [38-40]. The lower uptake observed below pH 3.4 may be attributed to the electrostatic repulsion between the protonated active sites on the sorbent and the positively charged uranyl species. The observed decrease in the uptake of UO_2^{2+} at pH $\geq$ 5.2 can be explained based on the formation of different uranyl species with lower adsorption affinities. The dependence of the uranium uptake on the pH value was further investigated by measuring the zeta potential. The surface zeta potential of the HOM-OCBBG sensor/captor was determined to be −21 mV (Fig. S1(E)). The negative value is due to the deprotonated groups (-OH, and $-NH_2$) of the HOM-OCBBG sensor/captor that can explain the pH variations of U(VI) ions uptake from solution by HOM-OCBBG sensor/captor.

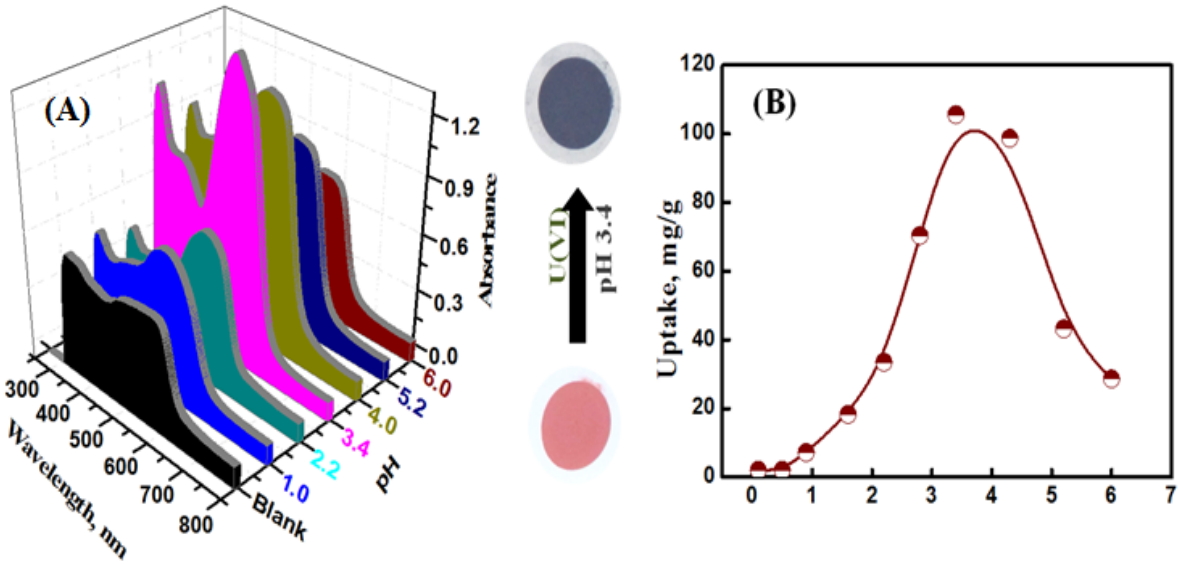

Fig. 4 (A) pH-dependence signal response of the uranyl-to-probe complex at 548 nm with the function of pH values. (B) Effect of pH on the removal/detection of U(VI) ions on HOM-OCBBG sensor/captor; initial U(VI) concentration 120 mg/L, weight of HOM-OCBBG sensor/captor 20 mg, solution volume 20 mL, contact time 30 min and 25 °C and inset is changes in color profiles during the detection/removal of U(VI) ions at 548 nm.

In general, the adsorption of U(VI) ions on the HOM-OCBBG optical sensor/captor proceeds through multi-steps including, bulk diffusion, film diffusion, pore diffusion, and interaction of U(VI) ions with OCBBG probe leading to the immobilization of adsorbed of species in the interior surface of pores [41]. To determine the rate-controlling step and shade more light on the kinetics of uranium-to-ligand binding, we first monitored the change in color and reflectance spectra of chromogenic OCBBG with time in 2 mg/L uranium solution (Fig. S3). Within the first ten minutes, the uptake of U(VI) ions reached 70.8% of its equilibrium value and reached equilibrium in 30 min (Fig.S4(A)). This fast removal of U(VI) ions reflects the fast kinetic of U(VI) ions on HOM-OCBBG, which outperforms that on other adsorbents reported in the literature. The kinetics of the adsorption process is further studied using several models. There is a satisfactory agreement between the calculated and the experimental values of q_e , and the regression coefficient (R^2) is close to 1, implying the adsorption proceeds following the pseudo-second-order model (Fig. S4(A) inset). Therefore, our results confirm that U(VI) adsorption on HOM-OCBBG results from the chemical interaction between the uranyl ions and the organic ligand. The results also indicate that the diffusion of uranyl ions controls the adsorption process's rate into the pores of the HOM-OCBBG sensor/captor (See Kinetic studied section in Supporting Information (Fig S4(A-C)).

The adsorption capacity of U(VI) ions on mesoporous captor/sensor as a function of the initial concentration is shown in Fig. S5(D&E). The adsorption curve indicates that the uptake of U(VI) ions increases with the initial concentration of the metal ion until a plateau at an uptake value of 95 mg/g. Thus, the uptake capacity of the sensor/captor is very high at low concentrations compared with that at high concentrations. The adsorption data were tested against Langmuir, Freundlich and Sips isotherms [42-44]. As shown in Fig. S5(D&E), the experimental data better fits Sip isotherm, and the regression coefficient is also higher than that calculated for other models. Using the Sip model, calculations were executed to obtain the predicted adsorption capacity of uranyl ions as a function of HOM-OCBBG weight for the specific uranyl ions concentrations. The value of HOM-OCBBG mesocaptor weight required to extract uranyl ions from 100 mg/L in 1 L solution volume to reach 1 mg/L was calculated to be 0.185 g/L.

3.3. Interaction between uranyl ions and HOM-OCBBG

The sensing mechanism and the ion adsorption behavior of U(VI) into HOM-OCBBG were further investigated by density functional theory (DFT) calculations. To simplify the computations, OCBBG was selected as a molecular model, which allows more focus on the sorption active sites rather than on the whole surface. Six uranyl complexes and OCBBG ligand structures were optimized at the DFT/B3LYP/LANL2DZ level, see Fig. 5 and supporting materials. Also, we considered the enolization of the OCBBG ligand. Details of these results are given and discussed in the supplementary materials. To explore the complexation mechanism of the uranyl ion and OCBBG ligand, six reactions were considered. As provided in Table S3 (Supporting Information), the change of Gibbs free energies (ΔG_{298}) of these reactions is negative. This implies spontaneous reactions. The most negative value is recorded for the reaction L + UO_2^{2+} + H_2O + NO_3^- → [$UO_2L(NO_3)$ (H_2O)] (-186.21 kcal/mol). Four of the six coordination sites in the equatorial plane around UO_2^{2+} are occupied by the tetradentate OCBBG ligand. The other two positions are insufficient to bind with another molecule of OCBBG. The complexes with the nitrate anion in the inner sphere are more favorable than those with a water molecule. The nitrate anion in the complex [$UO_2L(NO_3)_{bi}$] acts as a chelating agent in the inner sphere, which is more stable than [$UO_2L(NO_3)_{mono}$]. [$UO_2L(NO_3)(H_2O)$] was found to be more stable than [$UO_2L(NO_3)_{bi}$] by 10 kcal/mol. This might be attributed to the intermolecular hydrogen bond formed between a water molecule and a nitrate anion. It is clearly observed that the water and nitrate ligands both play essential roles in the sorption process. When water participates, the ΔG values increase to be more negative by 33 kcal/mol, while the coordination with one nitrate ion in [$UO_2L(NO_3)_{bi}$] increases ΔG_{298} to be more negative by 105

kcal/mol. Among all complexes, the $[UO_2L(NO_3)(H_2O)]$ is the most stable one as ΔG_{298} becomes more negative by 115 and 10 kcal/mol relative to $[UO_2\ L]^+$ and $[UO_2L(NO_3)_{bi}]$, respectively. To study the solvent's effect and obtain more reliable results, the interaction energies in water as solvent media were studied using the polarized continuum model (PCM). The solvation energies of the uranyl ion and its complexes were calculated using the following equation ($\Delta E_0 = E_{sol} - E_{gas}$). It was found that the solvation energy of the complexes are -95.7, -80.6, -76, -55.5, -61.8, and 16 kcal/mol for complexes 1-6, respectively, which is less negative than that of free uranyl ion (-373.3 kcal/mol) and indicates that the solubility of the free uranyl ion decreased after the complexation with the omega chrome black G. The positive value of the solvation energy of $[UO_2L(NO_3)\ (H_2O)]$ complex, which has the most negative binding energy, suggests the poor solubility of this complex. The water-insoluble complexes make it very easy to separate them from the reaction systems and allow the recycling and re-use of the sensor/captor.

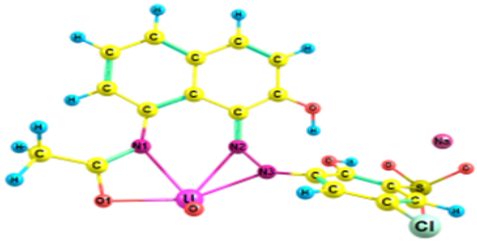

(1) $[UO_2\ L]^+$

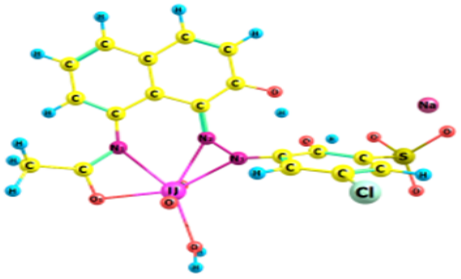

(2) $[UO_2L(H_2O)]^+$

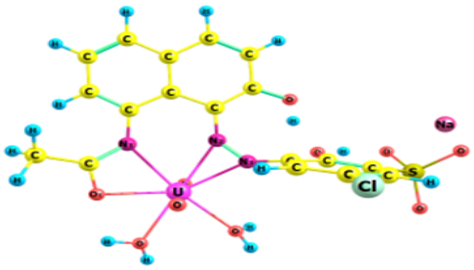

(3) $[UO_2L(H_2O)_2]^+$

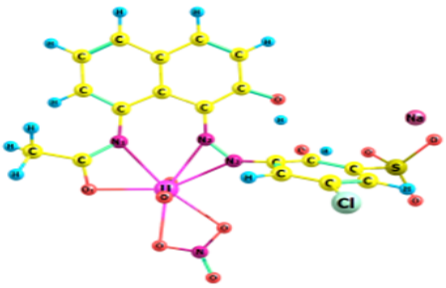

(4) $[UO_2L(NO_3)bi$

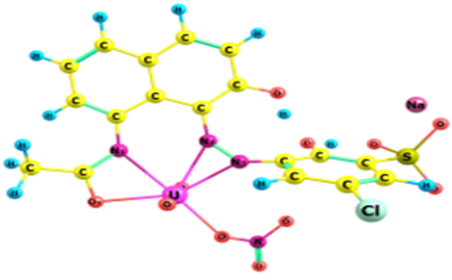

(5)$[UO_2L(NO_3)_{mono}]$

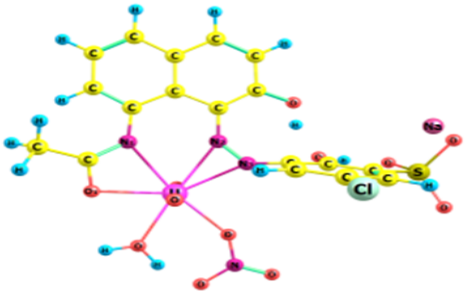

(6) $[UO_2L(H_2O)(NO_3)]$

Fig. 5 Optimized structures of the uranyl complexes

3.4 Sensor evaluation and limit of detection

Calibration of the click-sensing method of the optical sensor/captor is crucial to control the accurate detection and signaling strength of the U(VI) analyte. Several quantification measurements (≥10 times) were performed using a wide range of standard uranyl ion concentrations at the optimal sensing conditions. The calibration plots showed a linear correlation at low uranyl ions concentrations (Fig. 6). The color of the U(VI) solution is visibly changed after one minute of adding the HOM-OCBBG sensor/captor, suggesting the possibility of using HOM-OCBBG as a colored sensor for uranium in an aqueous environment. U(VI) detection sensitivity using HOM-OCBBG was performed using a simple and sensitive sequential quantification of the color of the sensor/solution suspensions with increasing the concentrations of U(VI) ions from 5 to 1000 µg/L. The reflectance spectra are collected to detect the changes associated with the OM-OCBBG -U(VI) ions interaction and the formation of the [HOM-OCBBG-UO_2] complex. The intensity of the peak at λ_{max} = 548 nm significantly increased with increasing the U(VI) ion concentrations (Fig. 6(A)). In addition, two extra peaks at around ~ 300 nm and 380 nm start to appear at U(VI) concentrations above 100 µg/L. Plotting the sensor response versus uranium content shows a linear relation at low concentrations, determining the LOD and QOD. D_R signifies the precise correlation of our experimental sensing procedure for the U(VI) ion-sensing data obtained from the synthesized HOM-OCBBG sensor/captor (5 to 1000 µg/L). The linear correlation at low concentration ranges indicates that uranyl ions can be detected and removed sensitively over a wide range of concentrations. However, a nonlinear correlation at the inflection point was evident at the highest concentration of uranyl ions (1000 µg/L). As can be seen for the inset of Fig. 6(B), the slope of the line is 0.026, and the standard deviation is SD = 0.079 (RSD% = 11.7 at n=10). Hence, the calculated LOD and QOD are 9.1 and 30.4 µg/L, respectively. These results imply that the mesoporous HOM-OCBBG sensor/captor can detect trace amounts of U(VI) in the solution. It should be mentioned here that the LOD of the HOM-OCBBG mesoporous sensor outperforms the published naked-eye sensor for U(VI) in contaminated seawater, comparable with that in freshwater, as shown in detail in Table S1 [1, 3, 6, 45-52]. The concept was used to develop sensor and analytical spectrophotometrical systems and improve the development of color (naked eye) detection. Table S1 in the supporting Information compares the performance of the cubically HOM-OCBBG mesocage sensor to others published in the literature, proving the outstanding properties of the new sensor. However, the detection limit of UO_2^{2+} is relative lower than that mesoporous thin film functionalized with silylated β-diketone [45] and

europium(III) organic framework [46] that gave LOD values of 1000 and 309.2 ug/L, respectively. Moreover, the loading of 2-(2-benzothiazolylazo)phenol (BTAP) and uranium(VI) anions into a plasticized cellulose triacetate matrix was illustrated for colorimetric detection of U(VI) from aqueous samples. The limit of detection was examined to be 160 μg/L at pH 6.5–7 in the presence of triethanolamine buffer [47]. Naked-eye detection of uranyl ions was also discussed in the case of Arsenazo III probe was immobilized on gold nanoparticles [21]. By taking advantage of the unique plasmonic properties of gold nanoparticles and the strong binding of arsenazo III with U(VI) ions, a photometric assay for uranyl ion was developed with a LOD of 119 μg/L detection limit. In contrast, Xu et al. [48] reported naked eyes sensor based on 1,3,5-triethynylbenzene and amidoxime/carboxylate conjugated microporous polymer with LOD of 0.4 μg/L. Also, an amidoxime-bearing sp^2 carbon-conjugated covalent organic framework was used for the detection of U(VI) ions from radioactive wastewater [49], with LOD of 1.5 ug/L. Qin et al. [50] reported a zinc-based metal-organic framework (HNU-50) with LOD is 2.8 μg/L for U(VI) ions in standard solution. Cui et al. [51] reported a sp^2 carbon-conjugated fluorescent covalent organic framework synthesized by integrating triazine-based building blocks with amidoxime-substituted linkers that showed good UO_2^{2+} detection of 1.6 μg/L. Most of these reported materials showed limited selectivity or stability, which couldn't be utilized for real application. It should be noted here that the concentration limit for uranium in seawater is approximately 3−9 μg/L. This means that our synthesized sensor is not sufficient for achieving natural levels and separation of uranium from seawater and is applied only on uranium-contaminated seawater [1]. The value of LOD (9.1 μg/L), far below the maximum contamination standard (30 μg/L) in drinking water defined by the United States Environmental Protection Agency (EPA), makes HOM-OCBBG material as a good candidate to achieve this goal and is still promising for the application in high level contaminated areas [3].

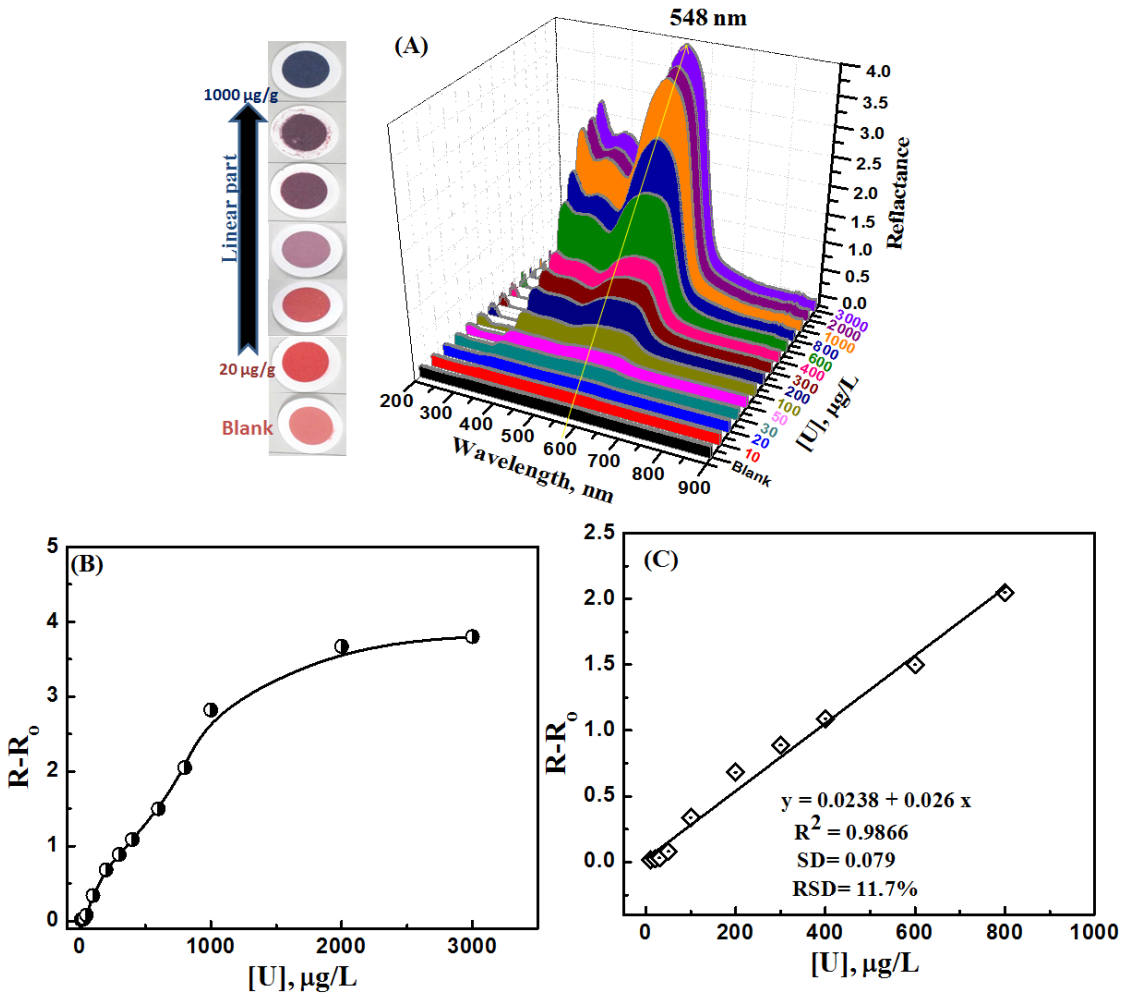

316

317 **Fig. 6** Effect of U(VI) concentration on (A) the reflectance spectra response of the HOM-OCBBG optical
318 sensor/captor at λ_{max}=548 nm, and (B) the calibration curve at λ_{max}=548 nm; pH=3.4; T=25 °C; t=20 min. (C) The
319 magnified section of the linear part of the graph at low concentrations.

320 **3.5 Selectivity assay**

321 The effects of the interfering ions on uranyl ions-selectivity of the optical sensor/captor were investigated by
322 studying each interfering metal ion's effect separately (binary system) and collectively (i,e, in a group of metals
323 ions) (Fig. 7). In binary-system, the interfering cations were initially added at various concentrations range to the
324 sensor/captor in uranyl-sensing conditions of pH and contact time. The initial concentration of the competing ions
325 used in this study is 1000 µg/L in binary mixtures of Th(IV), Dy(III), Nd(III), Pr(III), Tb(III), Er(III), Eu(III),
326 Sm(III), Ho(III), Yb(II), Fe(III), Al(III), Cu(II), Ag(I), Na(I), Mg(II), Ca(II), V(III), Co(II), and Ni(II) (Fig. 7(A-

C)). In a multi-component system, the effect of the competing ions on the uranyl ion-selective optical sensor/captor was investigated by studying the uranyl ions sensing selectivity from mixtures of different metal ions at its optimal sensing conditions. The content of each group of multi-component ions samples mixed with 1000 µg/L of uranyl ions includes, S-1: Th(IV), Yb(III), Na(I), Ca(II); S-II Dy(III), Nd(III), Pr(III), Tb(III); S-III: Er(III), Eu(III), Sm(III), Ho(III); S-IV: Y(III), Cd(II), Cs(I), Sr(II); S-V: Fe(III), Al(III), Cu(II), Mg(II); S-VI: Li(I), V(III), Co(II), Ni(II); S-VII: Bi(III), Ti(IV), Zr(IV), Hf(IV); S-VIII: Au(III), Ag(I), Pd(II), Ru(II) and G-IX: Cd(II), Pb(II) , Hg(II), Zn(II) (Fig. 7D). The competitive actinides and lanthanide ions are present (Fig. 7(A&B)). The co-existence of heavy metal ions could also reduce the sensitivity toward uranyl ions, especially in the case of Fe(III) and Al(III) ions. Fig. 7(A) shows the color changes of HOM-OCCBG monolithic strips at the optimal sensing conditions with various interfering ions. Clearly, only uranium ions are causing color changes when interacting with the OCCBG sensor/captor with slight change with thorium ions that gradually increased with increasing the pH value. The selectivity of the optical sensor/captor can be ascribed to its high binding affinity for the uranyl ions at the optimal ion-sensing conditions and the stability of the formed $[U\text{- OCCBG}]^{n+}$ complex. This result shows fast binding interactions and the stability of the target metal-to-L complex on the pore surfaces under optimal pH conditions, leading to the selective visual detection of U(VI) ions in aqueous samples. The stability constant (*log Ks*) of the formed $[U\text{-}L]^{n+}$ complex at a specific pH value significantly affects the uranyl ion-selectivity of the fabricated sensor/captor, particularly at low metal ions concentration compared with competitive matrices. The value of *log* $K_{U(VI)}$ can be calculated using the following equation: $\log K_{U(VI)} = [ML]_S / [L]_S \times [M]$, where *[M]* refers to the concentration of free unreacted uranyl ions, *[L]* represents the concentration of the organic ligand attached to the inorganic carrier and S refers to species in the solid phase [10, 32]. The results from the binding constants (*log* $K_{U(VI)}$) of the complex formed upon addition of uranyl ions of 6.75 at pH 3.4, indicating that the O/N-containing ligand binds strongly to the U(VI) ions onto the sensor/captor surface. In general, the U(VI)-L binding affinity onto the sensor/captor pore surfaces was due to the intrinsic mobility of the immobilized ligand to bind the uranyl ions efficiently in these sensing systems.

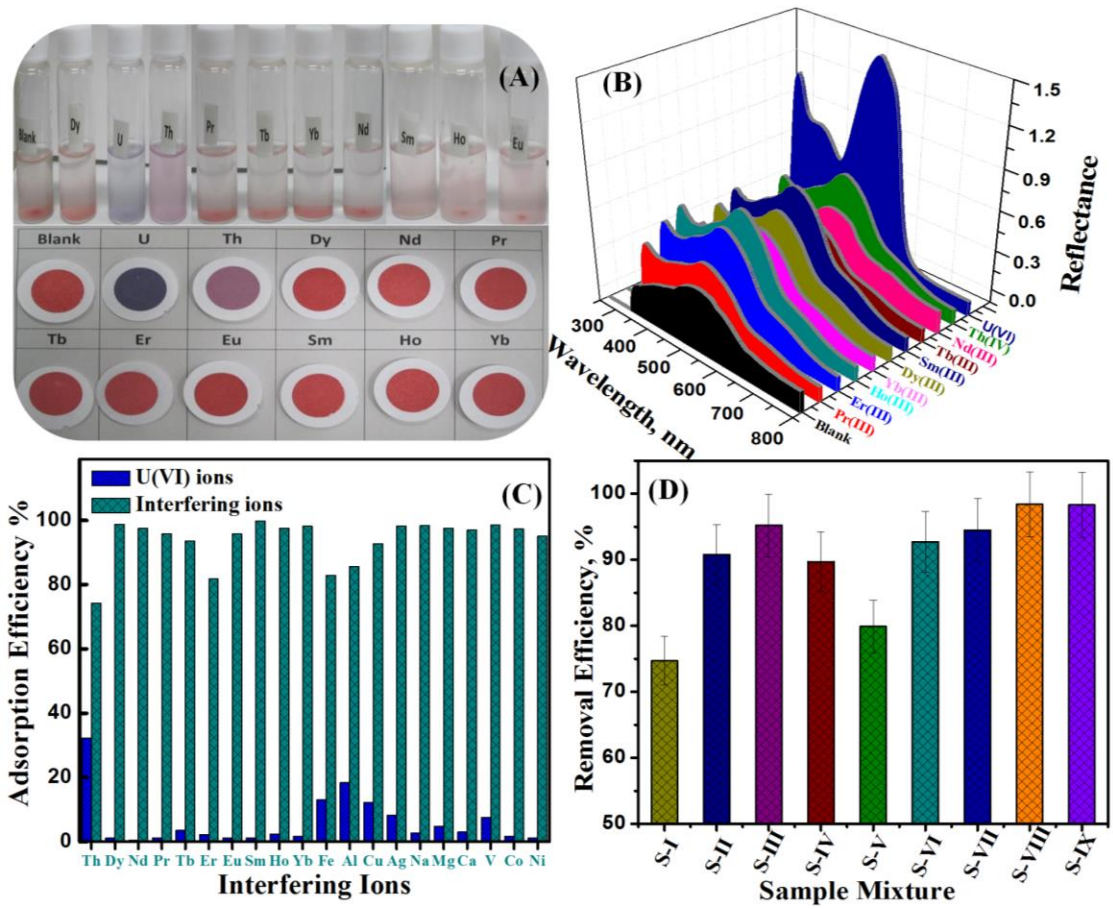

Fig. 7(A) Color response profile observed for HOM-OCBBG monolithic strip, when equilibrated individually with various lanthanides and actinides at pH value of 3.4, with [1000 µg/L] metal ions at a temperature of 25°C and, (B) pH-dependent selectivity UV measurements in the presence of other interfering species. (C) ICP-MS analysis U(IV) ions, where interfering ions are individually added to the U(VI) ions. (D) Separation of U(VI) ions from group mixtures of different metal ions using HOM-OCBBG at the optimal experimental condition.

3.6 Application with a real water sample

To validate the practicality of the mesocage HOM-OCBBG sensor/captor was used for the quantitative and qualitative detection of U(VI) ions in real uranium-contaminated seawater samples along with the selective removal, where competing ions are also present in the system. The compositions of the seawater samples are shown in Table S1. The accuracy of the proposed procedure was investigated by conducting recovery experiments on seawater samples by injecting a known quantity of U(VI) (500 µg L^{-1}) into the analyzed matrix. A series of batch experiments were performed to define and evaluate the specific removal and detection of U(VI) ions from real seawater (502 µg/L U(VI)) after adjusting the pH at 3.4. The uranium ion sensing/adsorption assays were performed under optimal

conditions. Despite the high concentration of competitive ions, the removal efficiency of U(VI) ions with the optical sensor/captor reach around 95%. This result indicates that the optical HOM-OCBBG sensor/captor is highly selective toward U(VI) ions even in the presence of high concentrations of competing ions in seawater. The main disadvantage of our method is the detection of uranium in real samples, while it requires adjusting the pH value of the samples at the desired pH.

3.7 Sensor/captor regeneration

The regeneration capability of the HOM-OCBBG mesocaptor was evaluated through submerging 100 mg of the HOM-OCBBG mesocaptor in 100 mL solution containing 50 mg/L uranyl ions at the optimal experimental conditions (time 20 min; pH 3.4 at 25°C). The solution was filtered, and the uranium loaded HOM-OCBBG mesocaptor was washed with DIW, and then eluted with HNO_3 for 30 min. The recovery efficiency (R_E %) was obtained from Eq. (2);

$$R_E\,(\%) = q_2 / q_1 \times 100 \qquad (2)$$

Where (R_E) is recovery efficiency (%), while q_1 and q_2 are the uptake of the 1st and 2nd run, respectively. Figure 8 compares the sorption and desorption efficiencies for the recovery of U(VI) for eight successive cycles, using 0.4 M HNO_3 solution as the stripping agent. The effective regeneration of the mesosensor under study was found feasible using 0.4 M HNO_3. HOM-OCBBG mesosensor was maintained up to the sixth cycle of regeneration, after which a subtle decrease in efficiency was observed, as shown in Fig. 8. The elution process offers notable stability for the first sixth cycle: the sorption efficiency gradually decreases from 95 to 74.3%, while desorption efficiency decreases from 99.2 to 87% from the first run. This sudden drop resulted from the partial leaching/dissolution of OCBBG organic film from silica nano-channels after successive cycles of adsorption/desorption in acidic media. After the fifth cycle, the loss in the efficiencies dramatically decreases, especially at the seventh cycle: sorption efficiency decreases to 68%, and the desorption efficiency tends to 64.9%, which specifies high durability and recoverability.

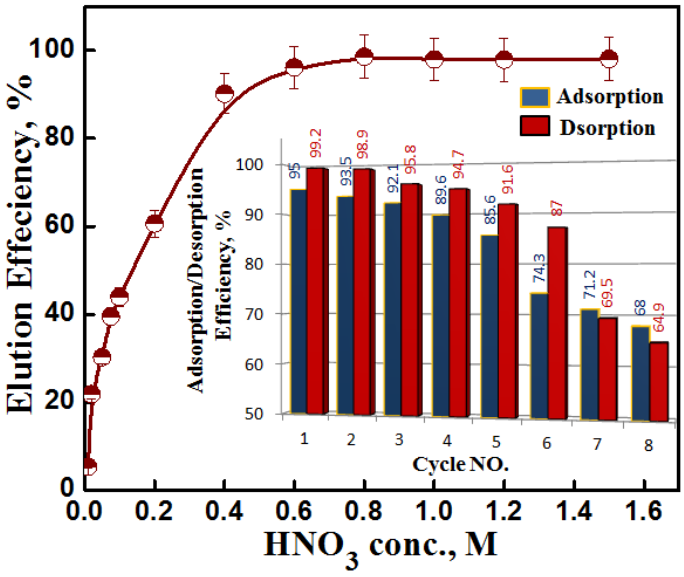

Fig. 8. Recyclability of HOM-OCBBG optical sensor/captor using different concentrations of HNO_3 and multiple re-use cycles of sorption/desorption (inset).

4. Conclusions

This study describes the development of nanostructured high ordered silica monolith decorated with OCBBG (HOM-OCBBG) for sensing and removing U(VI) ions from contaminated water. The mesoporous silica carrier was fabricated by using a quaternary microemulsion liquid crystalline phase based on a direct template with a high-ordered structure and large surface-to-volume ratios (412 m2/g and 0.841 cm3/g, respectively). Benefiting from the high surface area, facial interaction between OCBBG and the U(VI) ions, the prepared composite reached a maximum capacity of 95 mg/g within 30 minutes of the sorption process, outperforming other sorbents in the literature. Furthermore, it was possible to recover the sorption capability of the composite 7 times with simple leaching, adding more advantages to HOM-OCBBG sorbent. As a sensor, HOM-OCBBG showed visible color change with U(VI) ions concentration, allowing fast naked-eye detection of the radioactive contamination. Quantitively, the newly designed sensor could detect uranium in aqueous solutions with LOD close to 9.1 µg/L while the LOQ approaches 30.4 µg/L. Therefore, the new design for the HOM-OCBBG that allows detecting and removing nuclear waste in one step could open the door for fast remediation of contaminated water.

References

1. Khamirchi R, Hosseini-Bandegharaei A, Alahabadi A, Sivamani S, Rahmani-Sani A, Shahryari T, Anastopoulos I, Miri M, Trang HN (2018) Adsorption property of Br-PADAP-impregnated multiwall carbon nanotubes towards uranium and its performance in the selective separation and determination of uranium in different environmental samples, Ecotoxicol. Environ. Safe., 150:136-143.
2. Rashad M, El-Sayed I, Galhoum A, Abdeen M, Mira, Elshehy EA, Zhang S, Lu X, Xin J, Guibal E (2021) Synthesis of α-amino phosphonate based sorbents–Influence of inserted groups (carboxylic vs. amine) on uranyl sorption, Chem. Eng. J., 421: 127830.
3. Liu W, Dai X, Bai Z, Wang Y, Yang Z, Zhang L, Xu L, Chen L, Li X, Gui D, Diwu J, Wang J, Zhou R, Chai Z, Wang S, (2017) Highly Sensitive and Selective Uranium Detection in Natural Water Systems Using a Luminescent Mesoporous Metal-Organic Framework Equipped with Abundant Lewis Basic Sites: A Combined Batch, X-ray Absorption Spectroscopy, and First Principle Simulation Investigation. Environ. Sci. Technol. 51(7): 3911-3921.
4. Elshehy EA, (2017) Removal of uranium ions from liquid radioactive waste using modified aluminosilica. Sep. Sci. Technol. 52(11): 1852-1861.
5. Tag El-Din A, Elshehy EA, El-Khouly M (2018) Cellulose Acetate/EDTA-Chelator Assisted Synthesis of Ordered Mesoporous HAp Microspheres for Efficient Removal of Radioactive Species from Seawater, J. Env. Chem. Eng. 16: 5845.
6. Hosseini S-H, Rahmani-Sani A, Jalalabadi Y, Karimzadeh M, Hosseini-Bandegharaei A, Kharghani K, Allahabadi A (2015) Preconcentration and determination of ultra-trace amounts of U(VI) and Th(IV) using titan yellow impregnated Amberlite XAD-7 resin, Int J. Environ Anal. Chem ., 95 : 277-290.7.
7. Sompalli, N.K., Deivasigamani, P. (2021) Fabrication of target specific solid-state optical sensors using chromoionophoric probe–integrated porous monolithic polymer and silica templates for cobalt ions. Anal Bioanal Chem 413; 3177–3191.
8. García J M., García FC., Serna F, de la Peña J L (2011) Fluorogenic and Chromogenic Polymer Chemosensors. Polymer Reviews 51; 341-390.
9. Yang H, Qi D, Chen Z, Cao M, Deng Y, Liu Z, Shao C, Yang L (2021) A Zn-based metal–organic framework as bifunctional chemosensor for the detection of nitrobenzene and Fe^{3+}, Journal of Solid State Chemistry, 296: 121970.
10. Zaid OF, El-Said WA, Yousif, AM, Galhoum AA, Elshehy EA, Ibrahim, Guibal E, Synthesis of microporous nano-composite (hollow spheres) for fast detection and removal of As(V) from contaminated water. Chem. Eng. J. 390: 124439.
11. Parola S, Julián López B, Luís D. Carlos LD, Sanchez C (2016) Optical Properties of Hybrid Organic-Inorganic Materials and their Applications. Adv. Funct. Mater, 26(36): 6506-6544.
12. Boroujerdi R, Abdelkader A, Paul R (2020) State of the Art in Alcohol Sensing with 2D Materials. Nano-Micro Lett. 12: 33.
13. Hussein MA, Alamry KA, El Shishtawy RM, Elshehy EA, El-Said WA (2020) Nanoporous colorant sensors and captors for simultaneous recognition and recovery of gold from E-wastes. Waste Management, 116: 166-178.
14. El-Safty SA, Shenashen MA, Sakai M, Elshehy EA, Halada K (2015) Detection and recovery of palladium, gold and cobalt metals from the urban mine using novel sensors/adsorbents designated with nanoscale wagon-wheel-shaped pores. JoVE 106: e53044.
15. a) Yousif AM, Zaid OF, El-Said WA, Elshehy EA, Ibrahim IA (2019) Silica nanospheres-coated nanofibrillated cellulose for removal and detection of copper(II) ions in aqueous solutions, Industrial & Engineering Chemistry Research 58 (12): 4828-4837; b) Shenashen M, El-Safty S, Elshehy EA, Khairy M (2015) Hexagonal-Prism-Shaped Optical Sensor/Captor for the Optical Recognition and Sequestration of Pd II Ions from Urban Mines, Eur. J. Inorg. Chem., 2015: 179–191.
16. Steinberg I. M., Lobnik A., Wolfbeis O. S., Characterization of an optical sensor membrane based on the metal ion indicator Pyrocatechol Violet Sensors and Actuators B 90 (2003) 230–235
17. Oehme I., Wolfbeis O.S., Optical sensors for determination of heavy metal ions, Microchim. Acta 126 (1997) 177–192.
18. Lobnik A, Turel M, Urek SK (January 20th 2012). Optical Chemical Sensors: Design and Applications, Advances in Chemical Sensors, Wen Wang, IntechOpen, DOI: 10.5772/31534. Available from: https://www.intechopen.com/books/advances-in-chemical-sensors/optical-chemical-sensors-design-and-applications
19. Liang Y., He Y (2016) Arsenazo III-functionalized gold nanoparticles for photometric determination of uranyl ion. Microchim Acta 183: 407–413.
20. Jauberty L, Drogat N, Decossas J, Delpech V, Gloaguen V, Sol V (2013) Optimization of the arsenazo-III method for the determination of uranium in water and plant samples. Talanta 115:751–754.

21. M. Khan, P. Warwick, N. Evans N (2006) Spectrophotometric determination of uranium with arsenazo-III in perchloric acid. Chemosphere 63:1165–1169.
22. Abd EL Rahman AA., Amin A, Osman FA. (1959) Omega chrome black blue G as a colorimetric reagent for the microdetermination of various cations. Z. Anal. Chem., 169: 420–431.
23. Vivero-Escoto JL, Carboni M, Abney C, deKrafft K, Lin W (2013) Organo-functionalized mesoporous silicas for efficient uranium extraction. Microporous Mesoporous Mater. 180:22-31.
24. Mir SH, Nagahara L, Thundat T, Mokarian-Tabari P, Furukawa H, Khosla A (2018) Review-Organic-Inorganic Hybrid Functional Materials: An Integrated Platform for Applied Technologies. J Electrochem Soc, 165(8): B3137-B3156.
25. Walcarius A, Mercier L (2010) Mesoporous organosilica adsorbents: nanoengineered materials for removal of organic and inorganic pollutants. J. Mater. Chem., 20(22): 4478-4511.
26. Abdelmageed N, El-Said WA, Younes AA, Atrees MS, Farag AB, Elshehy EA, Abdelkader AM (2021) Facile synthesis of silica-polymer monoliths using nonionic triblock copolymer surfactant for efficient removal of radioactive pollutants from contaminated seawater. J Appl Polym Sci. e51263.
27. El-Said W. A., El-Khouly M. E., Ali M. H., Rashad R. T., Elshehy E. A., Al-Bogami A. S., J. Environ. Chem. Eng., 2018, 6(2), 2214-2221. b) Hussein M. A., Alamry K. A., El Shishtawy R. M., Elshehy E. A., El-Said W.A., Waste Manage., 2020, 116, 166–178.
28. Nazmul Hasan Md., Shad Salman Md., Islam A, Znad H, Munjur Hasan Md., Sustainable composite sensor material for optical cadmium(II) monitoring and capturing from wastewater, Microchemical Journal, 161, 2021,105800
29. W. A. El-Said, M. E. El-Khouly, M. H. Ali, R. T. Rashad, E. A. Elshehy, A. S. Al-Bogami, J. Environ. Chem. Eng., 2018, 6(2), 2214-2221.
30. Das T, Roy A, Uyama H, Roy P, Mahasweta, Nandi M, 2-Hydroxy-naphthyl functionalized mesoporous silica for fluorescence sensing and removal of aluminum ions, Dalton Trans., 2017, 46, 7317-7326
31. El-Safty, S. A.; Shenashen, M. A.; Sakai, M.; Elshehy, E.; Halada, K., Detection and recovery of palladium, gold and cobalt metals from the urban mine using novel sensors/adsorbents designated with nanoscale wagon-wheel-shaped pores. JoVE (Journal of Visualized Experiments) 2015, (106), e53044.
32. Elshehy, E. A.; Shenashen, M. A.; Abd El-Magied, M. O.; Tolan, D. A.; El-Nahas, A. M.; Halada, K.; Atia, A. A.; El-Safty, S. A., Selective Recovery of Silver (I) Ions from E-Waste using Cubically Multithiolated Cage Mesoporous Monoliths. European Journal of Inorganic Chemistry 2017, 2017 (41), 4823-4833.
33. Sonin DL, Korolev DV, Postnov VN Naumysheva E, Pochkaeva EI, Vasyutina ML, Galagudza MM, (2016) Silicon-containing nanocarriers for targeted drug delivery: synthesis, physicochemical properties and acute toxicity. Drug Delivery 2016. 23(5): 1747-1756.
34. A. S.Abdel-Bary, D.A.Tolan, M. Y.Nassar, T. Taketsugude, A. M. El-Nahas, (2020) Chitosan, magnetite, silicon dioxide, and graphene oxide nanocomposites: Synthesis, characterization, efficiency as cisplatin drug delivery, and DFT calculations, Int. J. Biol. Macromol. 154:621-633.
35. Deng L, Fang H, Zhang P, Abdelkader A, Ren X, Li, Y, Xie N (2016) Nitrogen and sulfur dual-doped carbon microtubes with enhanced performances for oxygen reduction reaction. **163**(5): H343.
36. Payne, KJ, Veis A, (1988) Fourier transform IR spectroscopy of collagen and gelatin solutions: deconvolution of the amide I band for conformational studies, Biopolymers, 27: 1749-60.
37. Hudson, E.A., Terminello, L.J., Viani, B.E., Denecke, M., Reich, T., Allen, P.G., Bucher, J.J., Shuh, D.K., Edelstein, N.M., (1999) The structure of U^{6+}sorption complexes onver miculite and hydrobiotite. Clays Clay Miner. 47: 439-457.
38. Fasfous, I.I., Dawoud, J.N., (2012) Uranium (VI) sorption by multiwalled carbon nanotubes from aqueous solution. Appl. Surf. Sci. 259: 433-440.
39. Schierz, A., Zänker, H. (2009) Aqueous suspensions of carbon nanotubes: surface oxidation, colloidal stability and uranium sorption. Environ. Pollut. 157: 1088–1094.
40. Kilislioglu, A. (2003) The effect of various cations and pH on the adsorption of U(VI) on Amberlite IR-118H resin. Appl. Radiat. Isot. 58, 713–717.
41. McKay, G, Poots VJP (1980) Kinetics and diffusion processes in colour removal from effluent using wood as an adsorbent. J. Chem. Technol. Biotechnol. 30(1): 279-292.
42. Freundlich H. (1906) Über die adsorption in lösungen. Z. Phys. Chem., 1906, 57: 387.
43. Langmuir I. (1948) The adsorption of gases on plane surfaces of glass, mica and platinum. J. Chem. Am. Soc., 1918, 40: 1361-1403.
44. Jeppu, GP, Clement T (2012), A modified Langmuir-Freundlich isotherm model for simulating pH-dependent adsorption effects. J. Contam. Hydrol. 2012. 129: 46-53.

45. Liu W, Wang Y, Song L, Silver MA, Xie J, Zhang L, Chen L, Diwu J, Chai Z, Wang S. (2019) Efficient and selective sensing of Cu^{2+} and UO_2^{2+} by a europium metal-organic framework. Talanta 196: 515–522.
46. Nicole L, Boissière C, Grosso D, Hesemann P, Moreau J, Sanchez C (2004) Advanced selective optical sensors based on periodically organized mesoporous hybrid silica thin films. Chem. Commun., 2004, 2312-2313
47. Hassan N, Amin AS, (2017) Membrane optode for uranium(VI) preconcentration and colorimetric determination in real samples. RSC Adv., **7**: 46566-46574

48. Xu M, Wang T, Gao P, Zhao L, Zhou L, Hua D, (2019) Highly fluorescent conjugated microporous polymers for concurrent adsorption and detection of uranium, J. Mater. Chem. A, 7:11214-11222.

49. Li F-F, Cui W-R, Jiang W, Zhang C-R, Liang R-P, Qiu J-D (2020) Stable sp2 carbon-conjugated covalent organic framework for detection and efficient adsorption of uranium from radioactive wastewater, J. Hazard. Mater. 392: 122333.

50. Qin X, Yang W, Yang Y, Gu D, Guo D, Pan Q (2020) A Zinc metal−organic framework for concurrent adsorption and detection of uranium. Inorg. Chem. 59: 14, 9857–986

51. Cui WR, Zhang CR, Jiang W, Li FF, Liang RP, Liu J, Qiu JD (2020) Regenerable and stable sp2 carbon-conjugated covalent organic frameworks for selective detection and extraction of uranium. Nat Commun. 11(1):436.

52. Behbahani M, Salimi S, HS, Abandansaria, Omidi F, Salarian M, Esrafili A, (2015) Application of a tailor-made polymer as a selective and sensitive colorimetric sensor for reliable detection of trace levels of uranyl ions in complex matrices. RSC Adv., 5, 59912-59920.